PHYSICAL REVIEW B **77**, 104434 (2008)

Tailoring of magnetocaloric response in nanostructured materials: Role of anisotropy

Victorino Franco,[1] Kleber R. Pirota,[2] Victor M. Prida,[3] Antonio Maia J. C. Neto,[4,5] Alejandro Conde,[1] Marcelo Knobel,[4] Blanca Hernando,[3] and Manuel Vazquez[2]

[1]*Departamento Física de la Materia Condensada, ICMSE-CSIC, Universidad de Sevilla, P.O. Box 1065, 41080 Sevilla, Spain*

[2]*Instituto Ciencia Materiales de Madrid, (ICMM-CSIC), Cantoblanco, 28049-Madrid, Spain*

[3]*Departamento de Fisica, Universidad de Oviedo, Calvo Sotelo s/n 33007 Oviedo, Spain*

[4]*Instituto de Fisica Gleb Wataghin, UNICAMP, Caixa Postale 6165, 13083-970 Campinas, São Paulo, Brazil*

[5]*Departamento Fisica, Universidade Federal do Pará, Campus Universitário do Guamá, 66075-110 Belém, Para, Brazil*

(Received 16 October 2007; revised manuscript received 11 February 2008; published 25 March 2008)

The magnetocaloric response of an ensemble of oriented uniaxial magnetic objects, perpendicularly magnetized to their easy axes, for temperatures close to the blocking temperature is calculated with the aim of demonstrating that the control of the sample's microstructure makes up an effective way to tailor its magnetocaloric response. Coexisting positive and negative magnetocaloric effect (MCE) is found for a model material with a single magnetic phase transition. Both MCE regimes are controlled by the magnitude of the applied magnetic field. As a proof of concept, experimental results for arrays of self-assembled ferromagnetic nanowires embedded into highly ordered nanoporous anodic alumina templates are shown, suggesting the validity of the numerical calculations.

DOI: 10.1103/PhysRevB.77.104434 PACS number(s): 75.30.Sg, 75.75.+a, 81.07.−b

INTRODUCTION

The characterization of the magnetocaloric response of materials, i.e., the change of their temperature due to the application of a magnetic field, is nowadays a field of increasing research interest, as evidenced by the huge increase in the number of publications devoted to this subject (for recent reviews, the reader is addressed to Refs. 1–5). Although the magnetocaloric effect (MCE) is not new (it was discovered by Warburg[6] in 1881), the combination of the recent discovery of the giant magnetocaloric effect[7] and the perspectives of the application of MCE in room temperature magnetic refrigerators[8–10] accelerated the research efforts in this field. This refrigeration method, although not yet available in commercial appliances, offers numerous advantages over the conventional systems based on the compression expansion of gases, ranging from increased energetic efficiency to environmental benefits due to the avoidance of ozone depleting or green house related gases.

The research efforts concerning magnetocaloric materials can be classified in: (a) the search for higher performance materials and (b) reduction of materials cost. The first one is usually centered around rare earth alloys,[7,11,12] while the second is accomplished by substituting rare earth elements by transition metals.[13] More recently, soft magnetic amorphous alloys are getting an increasing attention as low cost candidates for magnetic refrigeration.[14–21]

From a more fundamental point of view, there are two particular aspects of research which should be remarked: (a) the study of the field dependence of MCE and (b) study of the role played by the microstucture of the sample in determining its magnetocaloric response. A deep understanding of both aspects can help in the optimization of the future refrigerator systems.[22] The first line of research is more mature, being approached from both experimental[23,24] and theoretical fronts (although usually restricted to a mean field approach[25,26]), with recent studies evidencing the existence of a universal curve for the magnetic entropy change of MCE materials, even when the mean field approach is not applicable.[27–29] The study of the influence of the material microstructure has been less developed and it also opens a broad range of possibilities. Most of the samples studied in the literature are polycrystalline. Single crystalline samples[30] were studied mainly to analyze the influence of the sample impurities. The influence of amorphicity on the MCE of specific materials was studied,[31] and a broadening of the magnetocaloric peak was observed due to disorder. The role of the size of the particles was also a subject of research, evidencing that superparamagnetic particles exhibit an enhanced magnetocaloric response with respect to their bulk counterparts.[32,33] From all these studies, it has been revealed that a carefully control of the sample microstructure can be used as a way of tuning the optimum magnetocaloric response of materials. However, no qualitative change in the behavior of the material is achieved: the magnetocaloric peak is displaced to other temperatures, broadened, or made sharper, but the shape of the curve remains essentially unchanged. For example, in the case of interacting superparamagnetic particles, the modellization of the behavior of the magnetization close to the order temperature can be made in a similar way to that of a ferromagnetic material close to the Curie temperature,[34] which explains the similarities of the magnetic entropy change curves obtained in both cases.[35]

However, the attention paid to the magnetic anisotropy and its influence on the MCE has been limited, being mainly centered on the magnetocrystalline anisotropy of monocrystalline samples.[36,37] In some cases,[36] it has been theoretically predicted that the exploit of anisotropy, by adequate sample rotation during the magnetization process, can be a method to enhance the refrigerant capacity of the material. However, it has to be considered that the anisotropy of nanostructured materials can, in principle, be tailored almost at will, being possible to control not only its magnitude but also the distribution of easy axes orientation (although not all types of materials allow the same degree of control). It is also worth

mentioning that close to the blocking temperature of a superparamagnetic system, the anisotropy is not fully overridden by thermal energy and has an influence on the shape of magnetization curves, which depart from the Langevin behavior.[38,39] The earliest studies on the influence of anisotropy on MCE for nanostructured materials concentrated only on moderately high applied magnetic fields.[40,41] However, already in these cases, a distortion of the magnetic entropy change dependence on the temperature could be observed.[40] Moreover, it will be shown that the low field dependence of MCE in some anisotropic nanomaterials can also exhibit a rich phenomenology.

The aim of this work is to evidence that a precise control of the magnetic anisotropy of a nanostructured material can lead to a magnetocaloric response that is qualitatively different to that of the bulk material. With the help of numerical simulation, we will show that an ensemble of uniaxial nanoobjects, being perpendicularly magnetized with respect to their easy axis, can exhibit a coexistence of positive and negative MCE for temperatures close to the superparamagnetic transition. The sign of the magnetic entropy change can be controlled by the maximum value of the applied magnetic field. As a proof of concept, experimental results obtained for highly ordered arrays of self-assembled ferromagnetic nanowires embedded into nanoporous anodic alumina templates having well-defined anisotropy easy axis are shown, suggesting the validity of the numerical calculations.

EXPERIMENT

Magnetic model

Let us consider a single domain particle having a well-defined uniaxial magnetic anisotropy. The energy of such a particle in the presence of an applied field of magnitude H can be written as

$$E = -\mu_0 M_s V H(\hat{e}_m \cdot \hat{e}_h) + KV(\hat{e}_m \wedge \hat{e}_k)^2, \tag{1}$$

where M_s is the saturation magnetization of the particle, V its volume, K is the anisotropy constant, and $\hat{e}_m$, $\hat{e}_h$, and $\hat{e}_k$ are the unit vectors along the directions of magnetization, applied magnetic field, and anisotropy axis, respectively. Dimensionless parameters can then be defined as

$$t = \frac{25kT}{2KV},$$

$$h = \frac{H}{H_K}, \quad H_K = \frac{2K}{\mu_0 M_S}, \tag{2}$$

where k is the Boltzmann constant. The blocking temperature is defined, as usual, as that connected to $1/25$ times the energy barrier,

$$T_B = \frac{\Delta E}{25k} = \frac{KV}{25k}. \tag{3}$$

When the particle temperature is increased above the blocking temperature, all the orientations of the magnetization of the particle (determined with the angles θ and ϕ with respect to the easy axis direction) acquire a non-negligible probability of occupation. The average value of the reduced magnetization ($m = M/M_S$) can be calculated as

$$\langle m \rangle = \frac{\iint e^{-E/kT}(\hat{e}_m \cdot \hat{e}_h)\sin\theta d\theta d\phi}{\iint e^{-E/kT}\sin\theta d\theta d\phi}, \tag{4}$$

producing superparamagnetic-like curves.

For temperatures below the blocking temperature, where the thermal energy causes a deviation of the moment orientation with respect to the zero temperature case (but not so important to eliminate the hysteresis), a Néel relaxation approach can be used which details are given elsewhere.[39] It has to be mentioned that the two-state approximation cannot be used in this case because although it can give information about the temperature dependence of coercivity, it cannot reproduce the influence of thermal activation on the shape of the magnetization curve and that information is required for the study of MCE.

The magnetization curves of uniaxial single domain particles perpendicularly oriented to the applied magnetic field have been numerically calculated, employing a resolution of 0.02 rad for both angles involved in the integration of Eq. (4), applied field values ranging from 0 to $10H_K$ with increments of $0.02H_K$, and temperatures from $0.02T_B$ up to $40T_B$.

Sample preparation

The fabrication of the honeycomb self-ordered nanoporous anodic alumina membranes (AAMs) was done following the two-step anodization process.[42] High purity aluminum (Goodfellow, 99.999%) foils were degreased, cleaned, dried and finally electropolished. The anodization procedure was done by using 0.3 M of oxalic acid solution as electrolyte. The anodization voltage was kept at 40 V and the electrolyte temperature at 2 °C. The first anodization time, which determines the final hexagonal ordering degree, was 24 h for all samples. After the first anodization, the formed porous aluminum oxide was removed by using a phosphoric acid solution. The patterns that remain printed on the aluminum surface then play the role of starting points for the porous growth during the second anodization process. The second anodization time was 2 h for all the samples, resulting in a total porous length of about 4.5 μm. The final alumina porous array, fabricated under the above conditions, presents a pore diameter of 35 nm and a distance between two adjacent pores of 105 nm, as schematically shown in Fig. 1.[43] The growth of highly ordered arrays of Ni and FeNi nanowires into the self-assembled pores of the AAM was carried out in a special homemade electrochemical cell by a pulsed electrodeposition method using the well-known Watts bath.[44] The electrodeposition time, which determines the nanowires length, was 2 h, resulting in 4500 nm long nanowires. During the electrodeposition, the temperature was kept at 40 °C. The pulsed electrodeposition method consists of a current pulse of minus 30 mA during 2 ms followed by a positive voltage pulse of 5 V also during 2 ms. After 1 s of

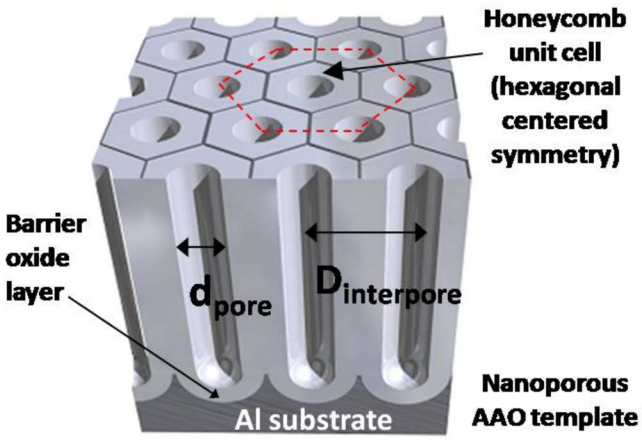

FIG. 1. (Color online) Sketch of a nanoporous AAM on aluminum substrate, showing the main parameters of the array: d_{pore} = nanopores diameter, $D_{\text{interpore}}$ = interpore spacing, and the unit cell of the nanoporous AAM, including also depicted the oxide barrier layer. Typical values are $d_{\text{pore}}=35$ nm and $D_{\text{interpore}}=105$ nm.

zero current and voltage, the previous pulse sequence is repeated again.[45]

Morphological studies were performed by high-resolution scanning electron microscopy (HRSEM) (LNLS, Brazil), revealing arrays of ferromagnetic nanowires highly ordered grown and uniformly aligned, with a diameter of 35 nm, arranged with hexagonal symmetry with a lattice constant (or internanowire distance) of 105 nm, as shown in Figs. 2(a) and 2(b). It is worth noting that there is no significant diameter distribution of the nanowires, as revealed in Fig. 2. In fact, in our case, we have an average pore diameter of 35 ± 2 nm, with a very narrow diameter distribution (less than 5%). The transmission electron microscopy (TEM) image shown in Fig. 2(c) reveals also the polycrystalline morphological structure of an isolated Ni nanowire.

The magnetization measurements were performed in a Quantum Design XL7 superconducting quantum interference device magnetometer in a temperature range between 4 and 300 K and applied magnetic fields up to 20 kOe. The magnetic response of the nanowire arrays was calculated by measuring separately (a) the as deposited ferromagnetic nanowires embedded in the alumina template and (b) the empty alumina matrix, and subtracting both signals. Figure 3(a) shows a magnetic force microscopy (MFM) image of a surface of $Ni_{69}Fe_{31}$ nanowires embedded into an AAM template in the remanence state. The dark and bright dots correspond to the magnetization, parallel aligned along the nanowires easy axes, pointing in opposite directions (upward or downward) due to the magnetostatic interactions among the nanowires in the remanent state.[46,47] Figure 3(b) shows a MFM image of a free standing Ni nanowire whose analysis denotes the essentially magnetic single domain structure of the nanowires. The nanowire shown in this image is identical to those ones considered in this work, i.e., a diameter of 35 nm and about 1000 nm length. The microscopy tip signal convolution gives as a result that the nanowire seems to be much wider than they actually are. The figure shows a dipolar magnetic monodomain configuration and there is no clear evidence of a more complex domain structure.

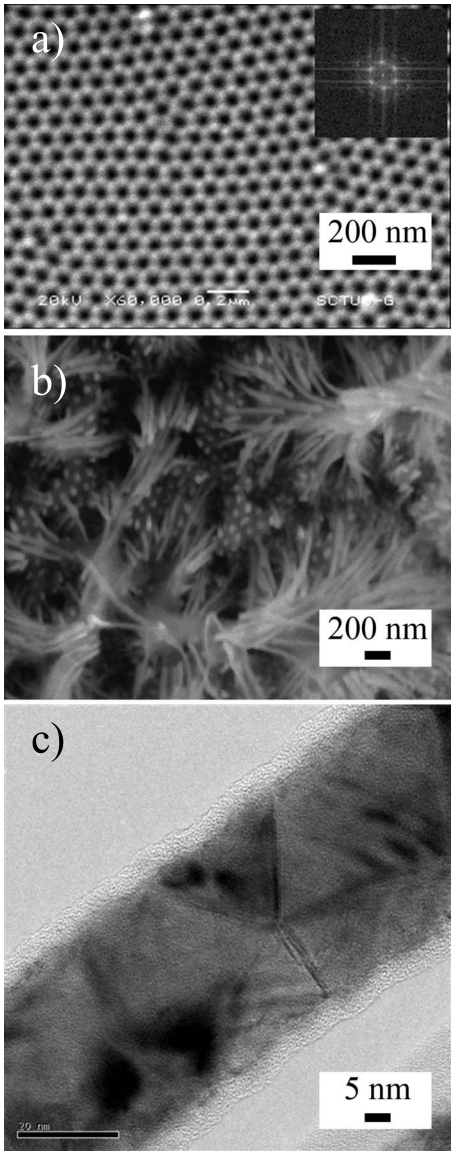

FIG. 2. (a) HRSEM image of an array of self-assembled nanoporous AAM template anodized in oxalic acid electrolyte in standard conditions described in the text. The high quality hexagonal self-ordered nanoporous structure is clearly unveiled in the FFT representation shown in the figure inset. (b) HRSEM image of an array of Ni nanowires after a partial dissolving of the alumina template with phosphoric acid etching. (c) TEM image of an isolated Ni nanowire showing its polycrystalline nanostructure.

RESULTS AND DISCUSSION

Figure 4 shows the calculated isothermal magnetization curves of a single domain particle with the magnetic field perpendicularly applied with respect to the easy axis for different temperatures below and above the blocking temperature. As indicated in a previous paper,[39] for moderately high applied magnetic fields, magnetization always decreases with increasing temperature. However, for low magnetic fields two different temperature regimes appear: at low temperatures, magnetization increases with increasing temperature, while at high temperatures magnetization decreases as tem-

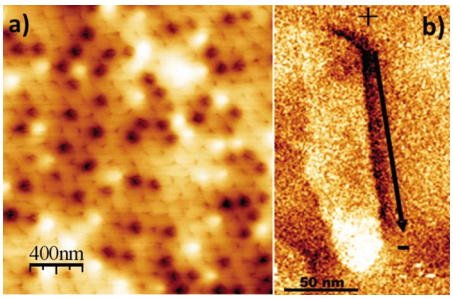

FIG. 3. (Color online) (a) MFM image of $Ni_{69}Fe_{31}$ nanowires arrays embedded into an AAM template in their remanent magnetic state. (b) MFM image of an isolated Ni nanowire showing its single-domain magnetic dipole structure. In this figure, the nanowire dimensions are 4 μm in length and 35 nm in diameter. The apparent higher aspect ratio is due to the microscopy tip convolution.

perature increases. This low field–low temperature increase of magnetization with increasing temperature, although not intuitive, can be explained by considering that some of the fluctuations of the magnetic moment would increase its projection along the direction of the applied magnetic field. This fact has the effect of increasing magnetization for a definite magnetic field and temperature intervals. Similar results were recently obtained by thermodynamical models.[48,49]

By using Maxwell relation, these numerically generated magnetization curves have been used to calculate the magnetic entropy change of an ensemble of identical uniaxial single domain nano-objects perpendicularly magnetized to their easy magnetization directions. In this way, the magnetic entropy change due to the application of a magnetic field H has been evaluated from the processing of the temperature and field dependent magnetization curves using a numerical approximation to the equation,

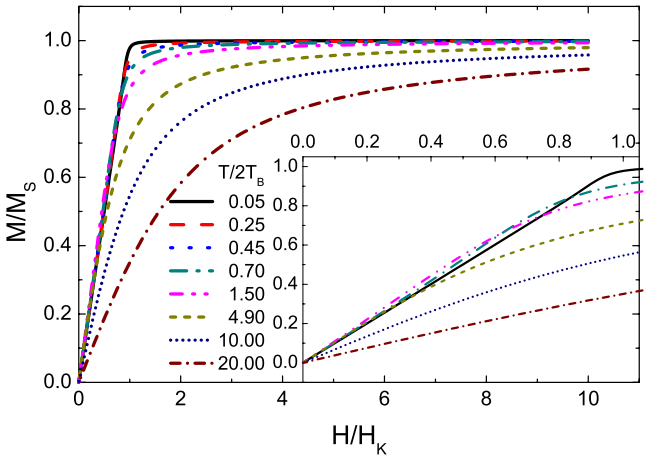

FIG. 4. (Color online) Field dependence of the isothermal magnetization curves of a single domain particle with the magnetic field perpendicularly applied with respect to the easy axis calculated for different temperatures. The inset shows a magnification of the low field region.

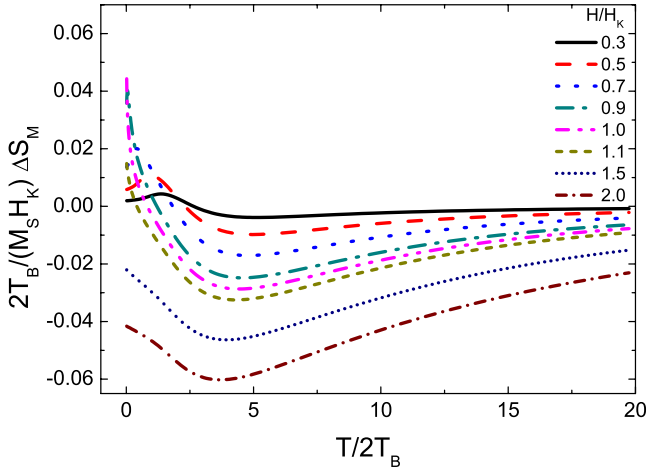

FIG. 5. (Color online) Temperature dependence of the magnetic entropy change for different values of the maximum applied field.

$$\Delta S_M = \int_0^H \left(\frac{\partial M}{\partial T}\right)_H dH, \tag{5}$$

where the partial derivative is replaced by finite differences and the integration is numerically performed.

Figure 5 shows the magnetic entropy change curves calculated from the magnetization curves in Fig. 4. For low applied fields, curves exhibit a positive ΔS_M peak (negative MCE) at low temperatures, and another negative ΔS_M peak (positive MCE) at high temperatures. By increasing the magnitude of the applied field, the magnitude of the high temperature peak also increases. The low temperature peak initially increases, shifting its position to lower temperatures, until it disappears. This behavior is in agreement with the one previously described for the temperature and field evolution of magnetization. The magnetic field dependence of the calculated ΔS_M curves is shown in Fig. 6. For low temperatures, the positive ΔS_M peak is located close to the an-

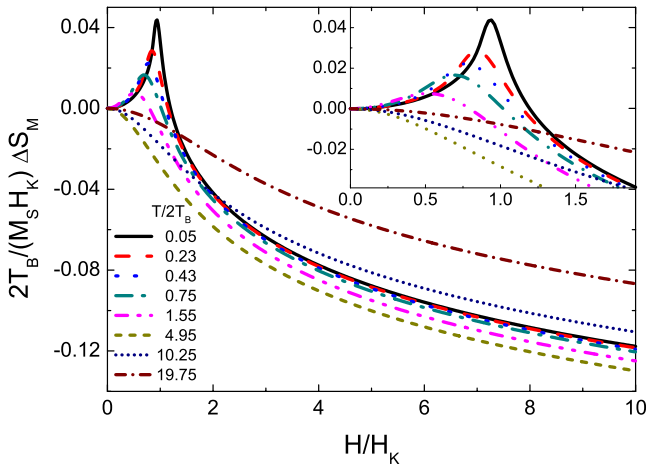

FIG. 6. (Color online) Field dependence of the magnetic entropy change for different temperature values. The inset shows a magnification of the low field region.

isotropy field. As temperature increases, the field associated with the maximum value of the entropy change shifts to lower values. This negative MCE effect is still detectable at temperatures close to $3T_B$. At all temperatures, high applied magnetic fields cause a progressive decrease of ΔS_M as temperature increases.

In a conventional ferromagnetic material close to the ferromagnetic to paramagnetic transition (Curie) temperature, $T \sim T_C$, magnetization decreases with increasing temperature, causing a negative magnetic entropy change when a magnetic field is applied [the argument of the integral of Eq. (5) is negative], which corresponds to a positive temperature increment of the material when magnetized (positive MCE). The situation gets more complicated for materials with a metamagnetic transition (from antiferromagnetic to ferromagnetic). In this case, the metamagnetic transition implies that magnetization increases when the transition temperature is overcome, which causes a positive peak in the magnetic entropy change and, therefore, a negative MCE. In this kind of materials, a coexistence of negative and positive MCE is also possible,[50] as the ferromagnetic to paramagnetic transition of the high temperature phase would imply a negative peak in ΔS_M. Even pure elements as Tb or Dy can exhibit combined positive and negative MCE due to their complicated phase diagram, with different magnetic transitions which are controlled by field or temperature.[51]

As far as we know, what is unique to the results presented in this work is that the coexistence of positive and negative MCE takes place for a material with a single magnetic phase transition and the nature of the magnetocaloric effect in this model system can be controlled by the magnitude of the applied magnetic field: for low applied magnetic fields and low temperatures, the material cools when magnetized, while for high magnetic fields the material heats when the field is applied. Therefore, a refrigeration device using such a material could change its operation mode at low temperatures just by changing the magnitude of the maximum applied magnetic field.

In order to test the practical feasibility of this predicted field controlled coexistence of positive and negative MCE, a material composed of uniaxial objects with parallel aligned easy axes has been measured. Therefore, arrays of highly ordered ferromagnetic nanowires were fabricated in self-assembled nanoporous AAM employed as templates. The magnetocrystalline anisotropy of the individual objects can be minimized by changing their composition. For this purpose, Permalloy (FeNi) and Ni nanowires were selected. Due to their geometry, the length to diameter aspect ratio of the nanowires makes the shape anisotropy, rather than the magnetocrystalline one, the most relevant contribution to the overall magnetic anisotropy of the sample. Therefore, the long and short wire directions, respectively, define the easy and hard magnetization easy axes of the arrays.[43] The temperature dependence of magnetization of the self-assembled Ni (main panels) and FeNi (insets) nanowires arrays measured with the magnetic field applied perpendicularly to the wires axes are shown in Fig. 7 [due to the small signal to noise ratio of the data, $M(T)$ curves for the Ni sample were smoothed with a Savitzky–Golay filter; for the Permalloy case, noise was reduced by selecting a smaller number of

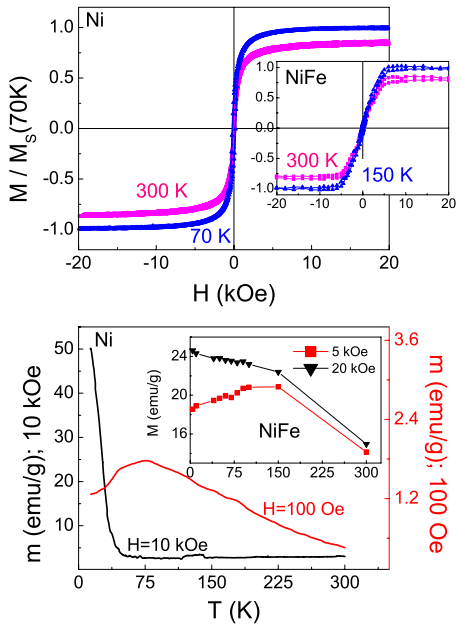

FIG. 7. (Color online) Lower panel: temperature dependence of magnetization for self-assembled Ni nanowires in AAM template measured with the magnetic field applied perpendicularly to the length of the nanowires. Upper panel: hysteresis loops (normalized with respect to the saturation magnetization at 70 K) of the Ni nanowires arrays with magnetic field applied perpendicular to the nanowires axis, which is measured at 300 and 70 K, respectively. The insets show the results for the NiFe nanowires.

experimental points just in the region of interest]. The applied fields were selected as one little under the anisotropy field of each of the samples and one well above it (100 Oe and 10 kOe for the Ni nanowires and 5 and 20 kOe for NiFe). The temperatures of the plotted hysteresis loops are room temperature and that corresponding to the maximum magnetization in the low field $M(T)$ curves (70 and 150 K for Ni and FeNi, respectively). The different values of the anisotropy field of each sample are in agreement with previously published experimental results.[52,53] These results are in good agreement with the magnetization models of Refs. 39 and 48, showing an increase in magnetization with increasing temperature for low temperatures and low applied magnetic fields, followed by a magnetization decreasing at higher temperatures. For high applied magnetic fields, magnetization continuously decreases as temperature increases. As explained above, this behavior is the reason for the coexisting negative and positive MCE predicted by the numerical simulations performed in this work. Therefore, it can be concluded that this particular behavior can be experimentally found for nanostructured systems having a well-defined uniaxial anisotropy. However, the low signal to noise ratio of the experimental measurements prevent any further calculation of the ΔS_M, as noise is enhanced by the numerical derivatives inherent to the calculations. Further efforts to increase the resolution of the measurements are being undertaken.

CONCLUSIONS

In conclusion, although the analyzed studies in which the magnetocaloric response of nanostructured magnetic materials indicate that the control of the microstructure is an effective way to tune the optimum performance of prospective refrigerant materials, in most of the cases, the shape of the temperature dependence of the magnetic entropy change is not altered, and the magnetocaloric response is qualitatively similar to that of the corresponding bulk materials. In this study, it has been shown that the adequate control of the magnetic anisotropy of a nanostructured system can originate behaviors which are qualitatively different from those of the bulk materials. In this way, apart from adjusting the composition of the material to tune its magnetocaloric response, the MCE of a particular sample can also be tailored by controlling its anisotropy. This fact can open new possibilities in the design of future applications of the magnetocaloric effect.

As an application of the previous concept, numerical simulations have been used to predict the coexistence of positive and negative magnetocaloric effects in a nanomaterial with a single magnetic phase transition: an ensemble of oriented uniaxial particles perpendicularly magnetized to their easy axes. It has been demonstrated that the coexistence of both MCE regimes can be controlled by the magnitude of the applied magnetic field. As a proof of concept, experimental magnetization curves for highly ordered arrays of self-assembled Ni and FeNi ferromagnetic nanowires embedded in honeycomb nanoporous alumina templates, whose magnetic properties are strongly dominated by the uniaxial shape anisotropy induced by the wires shape, have also been shown, evidencing the practical feasibility of the predicted behavior.

ACKNOWLEDGMENTS

This work was supported by the Spanish Government and EU-FEDER (Projects MAT2004-04618, MAT 2007-65227, MAT2006-13925-C02-01, and MAT2007-65420-C02-01), by the PAI of Junta de Andalucía (Project P06-FQM-01823), by FICyT (Projects FC04-EQP-28 and FC06-PC041), and by the Brazilian agencies FAPESP and CNPq. The authors acknowledge A. Asenjo, J. L. Baldonedo, and M. Jaafar for the TEM and MFM microscopy images.

[1] A. M. Tishin, in Handbook of Magnetic Materials, edited by K. H. J. Buschow (Elsevier, Amsterdam, 1999), Vol. 12, pp. 395–524.
[2] K. A. Gschneidner, Jr. and V. K. Pecharsky, Annu. Rev. Mater. Sci. **30**, 387 (2000).
[3] A. M. Tishin and Y. I. Spichkin, The Magnetocaloric Effect and Its Applications (Institute of Physics, Bristol, 2003).
[4] E. Bruck, J. Phys. D **38**, R381 (2005).
[5] A. M. Tishin, J. Magn. Magn. Mater. **316**, 351 (2007).
[6] E. Warburg, Ann. Phys. Chem. **13**, 141 (1881).
[7] V. K. Pecharsky and K. A. Gschneidner, Jr., Phys. Rev. Lett. **78**, 4494 (1997).
[8] C. A. Zimm, A. Jastrab, A. Sternberg, V. K. Pecharsky, K. A. Gschneidner, Jr., M. G. Osborne, and I. E. Anderson, Adv. Cryog. Eng. **43**, 1759 (1998).
[9] F. Shir, C. Mavriplis, L. H. Bennett, and E. Della Torre, Int. J. Refrig. **28**, 616 (2005).
[10] E. Brück, O. Tegus, D. T. C. Thank, and K. H. J. Buschow, J. Magn. Magn. Mater. **310**, 2793 (2007).
[11] V. Provenzano, A. J. Shapiro, and R. D. Shull, Nature (London) **429**, 853 (2004).
[12] T. Krenke, E. Duman, M. Acet, E. F. Wassermann, X. Moya, L. Mañosa, and A. Planes, Nat. Mater. **4**, 450 (2005).
[13] O. Tegus, E. Bruck, K. H. J. Buschow, and F. R. de Boer, Nature (London) **415**, 150 (2002).
[14] T. D. Shen, R. B. Schwarz, J. Y. Coulter, and J. D. Thompson, J. Appl. Phys. **91**, 5240 (2002).
[15] D. Wang, K. Peng, B. Gu, Z. Han, S. Tang, W. Qin, and Y. Du, J. Alloys Compd. **358**, 312 (2003).
[16] S. Atalay, H. Gencer, and V. S. Kolat, J. Non-Cryst. Solids **351**, 2373 (2005).
[17] S. G. Min, K. S. Kim, S. C. Yu, H. S. Suh, and S. W. Lee, J. Appl. Phys. **97**, 10M310 (2005).
[18] V. Franco, J. S. Blázquez, C. F. Conde, and A. Conde, Appl. Phys. Lett. **88**, 042505 (2006).
[19] F. Johnson and R. D. Shull, J. Appl. Phys. **99**, 08K909 (2006).
[20] V. Franco, J. M. Borrego, A. Conde, and S. Roth, Appl. Phys. Lett. **88**, 132509 (2006).
[21] V. Franco, C. F. Conde, A. Conde, and L. F. Kiss, Appl. Phys. Lett. **90**, 052509 (2007).
[22] V. K. Pecharsky and K. A. Gschneidner, Jr., Int. J. Refrig. **29**, 1239 (2007).
[23] V. K. Pecharsky and K. A. Gschneidner, Jr., Adv. Cryog. Eng. **42**, 423 (1996).
[24] S. Yu. Dan'kov, A. M. Tishin, V. K. Pecharsky, and K. A. Gschneidner, Jr., Rev. Sci. Instrum. **68**, 2432 (1997).
[25] H. Oesterreicher and F. T. Parker, J. Appl. Phys. **55**, 4334 (1984).
[26] For a comprehensive summary of the application to rare earth metals, see section 8.1.8 of Ref. 3.
[27] V. Franco, J. S. Blázquez, and A. Conde, Appl. Phys. Lett. **89**, 222512 (2006).
[28] V. Franco, J. S. Blázquez, M. Millán, J. M. Borrego, C. F. Conde, and A. Conde, J. Appl. Phys. **101**, 09C503 (2007).
[29] V. Franco, A. Conde, V. K. Pecharsky, and K. A. Gschneidner, Jr., Europhys. Lett. **79**, 47009 (2007).
[30] S. Yu. Dan'kov, A. M. Tishin, V. K. Pecharsky, and K. A. Gschneidner, Jr., Phys. Rev. B **57**, 3478 (1998).
[31] J. Sanchez Marcos, J. Rodriguez Fernandez, B. Chevalier, J. L. Bobet, and J. Etourneau, J. Magn. Magn. Mater. **272**, 579 (2004).
[32] R. D. McMichael, R. D. Shull, L. J. Swartzendruber, L. H. Bennett, and R. E. Watson, J. Magn. Magn. Mater. **111**, 29 (1992).
[33] P. Poddar, J. Gass, D. J. Rebar, S. Srinath, H. Srikanth, S. A. Morrison, and E. E. Carpenter, J. Magn. Magn. Mater. **307**, 227 (2006).

[34] S. Mørup and G. Christiansen, J. Appl. Phys. **73**, 6955 (1993).
[35] R. D. Shull, IEEE Trans. Magn. **29**, 2614 (1993).
[36] A. L. Lima, K. A. Gschneidner, Jr., and V. K. Pecharsky, J. Appl. Phys. **96**, 2164 (2004).
[37] P. J. von Ranke, N. A. de Oliveira, C. Mello, D. C. Garcia, V. A. de Souza, and A. M. G. Carvalho, Phys. Rev. B **74**, 054425 (2006).
[38] V. Franco and A. Conde, J. Magn. Magn. Mater. **277**, 181 (2004).
[39] V. Franco and A. Conde, J. Magn. Magn. Mater. **278**, 28 (2004).
[40] L. H. Bennett, R. D. McMichael, R. D. Shull, L. J. Swartzendruber, and R. E. Watson, J. Appl. Phys. **73**, 6507 (1993).
[41] L. H. Bennett, R. D. McMichael, H. C. Tang, and R. E. Watson, J. Appl. Phys. **75**, 5493 (1994).
[42] H. Masuda and K. Fukuda, Science **268**, 1466 (1995).
[43] V. M. Prida, K. R. Pirota, D. Navas, A. Asenjo, M. Hernández-Vélez, and M. Vázquez, J. Nanosci. Nanotechnol. **7**, 272 (2007).
[44] K. Nielsch, F. Müller, A.-P. Li, and U. Gösele, Adv. Mater. (Weinheim, Ger.) **12**, 582 (2000).
[45] K. R. Pirota, D. Navas, M. Hernández-Vélez, K. Nielsch, and M. Vázquez, J. Alloys Compd. **369**, 18 (2004).
[46] D. Laroze, J. Escrig, P. Landeros, D. Altbir, M. Vázquez, and P Vargas, Nanotechnology **18**, 415708 (2007).
[47] J. Escrig, D. Altbir, M. Jaafar, D. Navas, A. Asenjo, and M. Vázquez, Phys. Rev. B **75**, 184429 (2007).
[48] P. Vargas, D. Altbir, M. Knobel, and D. Laroze, Europhys. Lett. **58**, 603 (2002).
[49] P. Vargas and D. Laroze, J. Magn. Magn. Mater. **272-276**, e1345 (2004).
[50] D. H. Wang, C. L. Zhang, H. C. Xuan, Z. D. Han, J. R. Zhang, S. L. Tang, B. X. Gu, and Y. W. Du, J. Appl. Phys. **102**, 013909 (2007).
[51] For a comprehensive description, the reader can consult section 8.1 of Ref. 3.
[52] M. Vazquez, M. Hernandez-Velez, K. Pirota, A. Asenjo, D. Navas, J. Velazquez, P. Vargas, and C. Ramos, Eur. Phys. J. B **40**, 489 (2004).
[53] D. Navas, A. Asenjo, M. Jaafar, K. R. Pirota, M. Hernandez-Velez, R. Sanz, W. Lee, K. Nielsch, F. Batallan, and M. Vazquez, J. Magn. Magn. Mater. **290**, 191 (2005).